Korean J. Chem. Eng., 37(11), 1888-1898 (2020)
DOI: 10.1007/s11814-020-0614-2

pISSN: 0256-1115
eISSN: 1975-7220

A thermo-kinetic study on co-pyrolysis of oil shale and polyethylene terephthalate using TGA/FT-IR

Gamzenur Özsin*,†, Murat Kılıç, Esin Apaydin-Varol**, Ayşe Eren Pütün***, and Ersan Pütün****

*Bilecik Şeyh Edebali University, Faculty of Engineering, Department of Chemical Engineering, 11210, Bilecik, Turkey
**Eskişehir Technical University, Faculty of Engineering, Department of Chemical Engineering, 26555, Eskişehir, Turkey
***Anadolu University, Faculty of Engineering, Department of Chemical Engineering, 26555, Eskişehir, Turkey
****Anadolu University, Faculty of Engineering, Department of Materials Science and Engineering Engineering, 26555, Eskişehir, Turkey

(*Received 20 February 2020 • Revised 28 May 2020 • Accepted 12 June 2020*)

Abstract−This study explored the effects of polyethylene terephthalate (PET) blending during the pyrolysis of oil shale (OS). Dynamic pyrolysis and co-pyrolysis tests at heating rates in the range from 5 to 40 °C/min were carried out using a thermogravimetric analyzer (TGA) coupled to a Fourier transform infrared spectrometer (FT-IR) to determine the kinetic parameters of the process and for online detection of evolved gasses. Pyrolytic decomposition of OS included a multi-stage decomposition process, while PET decomposed only in a single step. The kinetics of pyrolysis and co-pyrolysis was determined via model-free iso-conversional methods, namely Friedman, FWO, Starink, Vyazovkin, in a conversion degree range of 0.1-0.9. The kinetic models were validated with the obtained data to describe pyrolytic and co-pyrolytic degradation mechanisms, and the regression coefficients were between 0.9823 and 0.9999. The results showed that the activation energy of co-pyrolysis was evidently lower than that of PET or OS pyrolysis. This led to the conclusion that co-pyrolysis could be a potential method for obtaining shale oil due to the synergy between OS and PET.

Keywords: Pyrolysis, Kinetics, PET, Oil Shale, Synergetic Effect, TGA/FT-IR

INTRODUCTION

Due to the accelerated industrialization and population growth, both energy supply and waste disposal by way of thermochemical processes are a prerequisite to solve the issues concerning sustainability [1]. For this purpose, research for waste to energy technologies, which may substitute conventional fossil energy resources, has intensified. As one of the most promising thermochemical conversion methods, pyrolysis converts a variety of carbonaceous materials to gaseous, liquid and solid fuels together with high-value added fine chemicals [2-4]. In pyrolysis technologies, organic materials such as low rank coals, biomass wastes, industrial and municipal sludge and polymeric wastes are potential precursors to produce synthetic fuels and chemical feedstock. Pyrolysis of oil shale (OS) has received attraction as a valuable energy source for many years for production of shale oil, which may be an alternative fuel for crude oil in the case of shortage of petroleum supply [5,6]. OS is an organic-rich sedimentary rock present on the surface of the earth. It includes a considerable amount of kerogen (10-65 wt% of the total mass) which can be converted into oil and a mineral porous matrix (including carbonates, clay and quartz) together with trace elements (As, B, Mo, Ni, Zn, Ti, etc.) [7-9]. The kerogen content of OS has a high H/C ratio, and hence, it has a considerable potential as a source of liquid fuel [10-12]. Approximately 15-20% of oil on average may be obtained from OS and extractable shale oil OS is estimated as 3 trillion barrels is known worldwide compared to 1.2 trillion barrels of crude oil known worldwide [13-15]. Therefore, attempts should be made for extraction of shale oil in an economical way to contribute to the future energy prospect of the world.

It is thought that co-processing OS with waste plastics during the co-pyrolysis may be a promising method to contribute to the protection of the environment by minimizing and disposing polymeric wastes [16,17]. This is because co-pyrolysis of single or mixed plastics may cause synergetic effects. The reasons behind co-pyrolysis include that hydrogen and radicals from polymers minimize production of hydrogen and hydrocarbon gases and increase oil yield [18-20]. A large number of previous studies have investigated co-pyrolysis of different OS samples with several synthetic polymers such as LDPE, HDPE and PP [10,21,22]. Based on the experimental findings, significant synergistic effects leading to higher product yields and improved product characteristics may be achieved by co-pyrolysis of OS with plastics. Although extensive experimental studies have been conducted on co-pyrolysis of OS and plastics in lab-scale systems, the kinetics of this process have been rarely reported. However, understanding the kinetics of pyrolysis and evolved gases are important criteria for effective operation of thermochemical conversion units together with their design, optimization and scaling up since pyrolysis makes up the first step of other thermochemical conversion processes such as combustion and gasification [23-25]. Moreover, kinetic parameter data is also necessary for the calculation of operating costs of thermochemical processes.

This study focused on investigation and comparison of decom-

†To whom correspondence should be addressed.
E-mail: gozsin@anadolu.edu.tr, gamzenur.ozsin@bilecik.edu.tr

position behavior, pyrolysis and co-pyrolysis kinetics of OS and PET in order to discuss their synergic effects, because co-pyrolysis of OS and PET has not been reported in the literature. Waste PET has a great potential for continuous hydrocarbon supply such as aromatics, polycyclic aromatic hydrocarbons, acids and esters and for synthetic fuel production [26-29]. Besides, studying co-pyrolysis of OS and PET is vital to enhance product yields and characteristics, as well as developing and designing new technologies for shale oil extraction. For this purpose, pyrolysis and co-pyrolysis characteristics were investigated using iso-conversional methods. Furthermore, simultaneous TGA/FT-IR analyses were performed to describe the interactions between OS and PET by gathering additional information on evolved gases.

MATERIAL AND METHODS

1. Properties of the Samples

PET samples were mainly disposable plastic bottles obtained from a local solid waste collection station which carefully separates plastics in place without contamination. As the PET plastic could not be milled in a high-speed cutting mill, the PET plastic was cut to small pieces that were then ground cryogenically. OS samples used in this research were obtained from Seyitömer region of Kütahya, Turkey. OS samples were also ground in a high-speed rotary cutting mill and homogenized. All samples were stored in transparent plastic containers and a particle size between 112 and 224 μm was used for TGA/FT-IR experiments. The particle size was selected to ensure that the Biot number was smaller than unity, which shows uniform temperature distribution inside the particle. To investigate the co-pyrolytic behavior of OS and PET and determine synergy between particles regardless of the blending ratio, samples were mixed at a fixed ratio as 1 : 1 (wt/wt) and mixed samples were named as PET/OS. Prior to thermoanalytical measurements ultimate and proximate analyses were carried out. Ash analysis of OS was also performed in order to quantify inorganic constituents using X-ray fluorescence spectroscopy (Rigaku XRF, ZSX).

2. TGA/FT-IR Experiments

Thermogravimetric analysis (TGA) is one of the most widely applied techniques to study pyrolytic thermal behavior of materials and thermochemical conversion processes like combustion, gasification and pyrolysis [30,31]. Combining TGA with different analytical techniques allows simultaneous investigation of volatile pyrolysis products [32]. As a common technique, TGA/FT-IR is useful in this sense. TGA/FT-IR experiments of the current study were performed using a TGA device (Setaram-Labsys Evo) that was coupled to an FT-IR spectrometer (Thermo Fisher-Nicolet iz10). A continuous nitrogen flow was supplied during the experiments and its flow rate was maintained at 20 cm^3/min. 10±0.1 mg of sample was weighted into an Al_2O_3 crucible. To correct the buoyancy effects, blank tests were also performed. Measurements of mass loss were monitored from 25 °C to 1,000 °C using linear heating rates from 5 to 40 °C/min.

While the weight loss of the sample was recorded, evolved gases from the TGA passed through an externally heated transfer line into the FT-IR gas cell. The transfer line between TGA and FT-IR was heated at 225 °C to prevent condensation of volatiles and dissociate all complexes. The background data was collected before each run. During simultaneous detection of volatiles with TGA, the IR cell was maintained at 250 °C and the spectra were recorded in the range of 400-4,000 cm^{-1}. With the software OMNIC, spectral analysis was done and reproducibility and accuracy of the gained data was confirmed.

3. Kinetic Analysis

Kinetic calculation involves measuring the amount of mass degraded versus the temperature at regular time intervals. TGA is an appropriate method for both characterization of the thermal behavior of fuels and predicts kinetics of the thermochemical conversion processes since it provides information on the decomposition rate as a function of time and temperature in a controlled environment [33-35]. For the TGA assays, the weight loss (TG) and the weight loss rate (dTG) were gained for pyrolysis and co-pyrolysis under inert atmosphere. During TG experiment, the mass of the sample was continuously measured as a function of temperature and time. Fractional conversion (α) at any time during pyrolysis can be defined by Eq. (1), where w_0, w_f and w_t are, respectively, the initial, final and the sample's instantaneous mass in the main decomposition zone. The conversion degree α reflects the progress of thermal decomposition:

$$\alpha = \frac{w_o - w_t}{w_o - w_f} \tag{1}$$

In thermal degradation of the structure using TGA, a pyrolysis reactivity index (R_p) in terms of [%·(min·mg)$^{-1}$] is calculated according to the following formula:

$$R_p = \frac{1}{w_o}\left(\frac{dw}{dt}\right)_{max} \tag{2}$$

where $(dw/dt)_{max}$ is the maximum pyrolysis rate and w_o is the initial weight before the pyrolysis stage. The fundamental of kinetic calculation based on the fact that conversion rate is proportional to the reactant concentration. Moreover, conversion rate during thermal degradation depends on temperature. In the case of constant heating rate (β), two different independent functions are used to express temperature dependency (k(T)) and fractional conversion (f(α)). By using these two equations, kinetic expression can be written as shown in Eq. (3):

$$\frac{d\alpha}{dt} = \beta\frac{d\alpha}{dT} = k(T)f(\alpha) \tag{3}$$

Commonly, the pyrolysis experiment is performed nonisothermally with a constant heating rate (β=dT/dt) and Arrhenius equation expresses temperature dependency by a calculation of the rate constant, k, [$k=Aexp(-E_a/RT)$] where E_a is the activation energy, A is the pre-exponential factor and R the gas constant. Hence, the reaction rate can be given in the form:

$$\beta\frac{d\alpha}{dT} = A\exp\left(-\frac{E_a}{RT}\right)f(\alpha) \tag{4}$$

where f(α) is the conversion function. Eq. (4) can be integrated into

$$\int_0^{\alpha}\frac{d\alpha}{f(\alpha)} = g(\alpha) = \frac{A}{\beta}\int_{To}^{T}\exp\left(-\frac{E_a}{RT}\right)dT \equiv \frac{AE_a}{\beta R}p(u) \tag{5}$$

Table 1. Linear model equations of model-free (iso-conversional) methods used in the study

Method	General form of equation	Basis of the method	Reference
Friedman	$\ln\left(\beta\frac{d\alpha}{dT}\right)=\ln A+\ln f(\alpha)-\frac{E_a}{RT}$	Assumes $f(\alpha)$ remains constant, degradation is independent of temperature and it depends only on the rate of mass loss.	[38]
FWO	$\ln\beta=\ln\frac{AE_a}{Rg(\alpha)}-5.331-1.052\frac{E_a}{RT}$	Assumes apparent activation energy remains constant during the degradation and Doyle approximation is applicable for mathematical formulation.	[39,40]
Starink	$\ln\left(\frac{\beta}{T^{1.8}}\right)=C_s-1.0037\frac{E_a}{RT}$	Assumes Flynn-Wall-Ozawa, Boswell and Kissinger-Akhira-Sunose methods are applicable and an optimisation among the models is performed.	[41]
Vyazovkin	$\sum_{i=1}^{n}\sum_{j\neq i}^{n}\frac{I(E_{a\alpha}, T_{\alpha,i})\beta_j}{I(E_{a\alpha}, T_{\alpha,j})\beta_i}=\min$	Assumes $g(\alpha)$ is independent of the heating program and non-linear regression proposed by Senum and Yang is used.	[42]

where $g(\alpha)$ and p(u) are known as the integrated forms of fractional conversion function, and temperature integral, respectively. p(u) does not have an exact analytical solution but it can be approximated by different empirical interpolation equations depending on the applied kinetic method. Generally, thermal decomposition processes are complicated processes which consist of hundreds of complex components and their parallel and/or consecutive reactions. For this reason, iso-conversional methods are suggested to interpret activation energy for the reliability and objectiveness by International Confederation for Thermal Analysis and Calorimetry (ICTAC) [36].

The basis of the iso-conversional approach is that the rate of decomposition is calculated by the current sample temperature at a certain point of conversion. Moreover, heating rate and temperature changes are considered as ineffective to the reaction mechanism [37]. To use iso-conversional methods, experiments at different heating rates have to be performed and Eq. (6) is acceptable:

$$\left[\frac{d\ln(d\alpha/dt)}{dT^{-1}}\right]_{\alpha}=-\frac{E_a}{R} \tag{6}$$

In the current study, the activation energy (E_a) was calculated by using model free iso-conversional methods: Friedman [38], FWO [39,40] Starink [41] and Vyazovkin [42]. The formula of each model is summarized in Table 1. For Friedman, FWO and Starink methods linear regression at each conversion degree was used for estimation of activation energy. On the other hand, the model equation was minimized by non-linear regression to calculate activation energy of each conversion degree for Vyazovkin method. Other than the activation energy distribution, reaction order was also determined by Avrami theory [43] as given in Eq. (7),

$$\alpha=1-\exp\left(\frac{-k(T)}{\beta^n}\right) \tag{7}$$

By taking the double logarithm of Eq. (7) and rearrangement of the equation, the last version can be rewritten as:

$$\ln(-\ln(1-\alpha))=\ln A-\left(\frac{E_a}{RT}\right)-n\ln\beta \tag{8}$$

Thus, plot of $\ln(-\ln(1-\alpha))$ versus $\ln\beta$ is established for the determination of the apparent reaction order (n).

RESULTS AND DISCUSSION

1. Characteristics of the Samples

OS and PET were characterized to have a better understanding of the correlation between fuel properties and their chemical structures. The results of ultimate, proximate and elemental analyses are summarized in Tables 2 and 3. According to the ultimate analysis, the ash content of OS seemed relatively high (66.5 wt%) in comparison to many ranks of coals. High ash content causes many problems, such as restrictions in mass and heat transfer by forming aggregations, which decrease the energy efficiency while processing OS alone. On the other hand, inorganics in OS ash have a desirable potential to undergo reactions such as cracking, dehydrogenation and coking when the oil phase vapor flows through a shale ash bed during large-scale operations [44]. These reactions are advantageous since they upgrade shale oil to generate an oil product

Table 2. Ultimate and mineralogical analyses of oil shale

Ultimate analysis (%)	
Moisture	5.57
Ash	66.50
Volatiles	19.87
Fixed carbon*	8.06
Ash analysis (%)	
SiO_2	48.7916
Fe_2O_3	20.7740
Al_2O_3	15.4376
MgO	3.9646
SO_3	3.1156
Na_2O	2.4266
CaO	2.3065
K_2O	1.6631
TiO_2	0.6765
MnO	0.3483
NiO	0.2241
P_2O_5	0.1648
Cr_2O_3	0.1068

*From difference

Table 3. Elemental composition of oil shale (OS) and PET (on dry-ash free basis)

	OS	PET
C (%)	83.78	61.62
H (%)	12.89	4.73
N (%)	1.07	0.26

with reduced heavy oil content [45]. Therefore, ash analysis was performed by XRF for quantitative determination of inorganic phases. The results showed that the main components of OS were SiO_2, Fe_2O_3 and Al_2O_3 which constitute more than 85 wt% of the inorganic phase. According to the proximate analysis results, PET had carbon and hydrogen content of 61.62 wt% and 4.7 wt%, respectively. The elemental composition or H/C ratio, which varies with the type of the plastic, affects the hydrogen donor mechanism and hence radical reactions during co-pyrolysis. Therefore, the presence of minor contamination of the precursors may alter the degree of the possible synergetic effects. On the other hand, volatile and fixed carbon content of PET was determined as 88.02 wt% and 11.98 wt%,

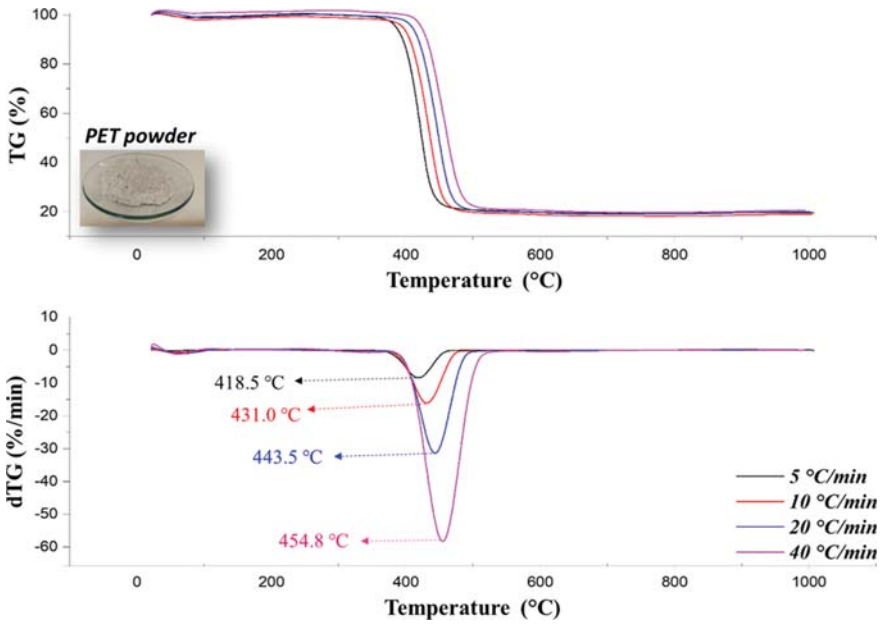

Fig. 1. Non-isothermal TG and dTG thermographs for PET pyrolysis at different heating rates.

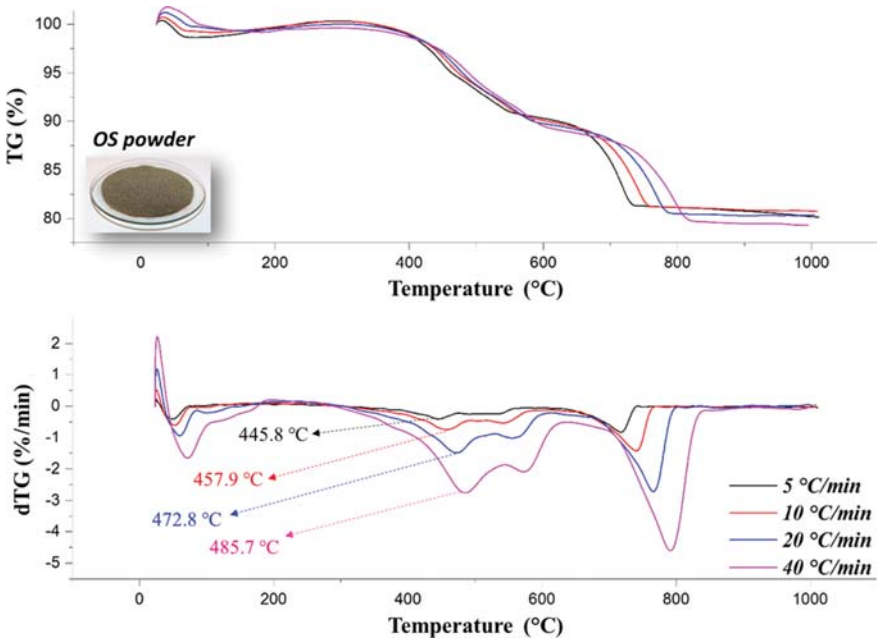

Fig. 2. Non-isothermal TG and dTG thermographs for OS pyrolysis at different heating rates.

respectively, while it had no moisture and ash in its structure.

2. TG and dTG Analysis

Comparison of pyrolysis and co-pyrolysis experiments performed in TGA for OS, PET and their blend could be made by thermogravimetry (TG) and derivative thermogravimetry (dTG) curves, which were recorded at several heating rates (Fig. 1-3). Furthermore, the pyrolysis and co-pyrolysis characteristics of the samples for each heating rate are given in Table 4 for a better numerical comparison. The mass loss patterns of the samples were almost the same at all heating rates, except for that little shift towards higher temperature observed at higher heating rate. When the heating rate increased from 5 to 40 °C·min^{-1}, a considerable lateral translation of the peaks towards to the higher temperature were observed. Thus, the onset and offset temperatures of the active pyrolysis region shifted to the higher temperatures. This is because of heat and mass transfer limitations which cause declined efficiency of heat transfer at higher heating rates than those at lower heating rates. This phenomenon is observed for various fuels since an increasing heating rate tends to postpone the thermal decomposition process, and the solid matrix breaks down at higher temperatures.

Pyrolysis of PET seemed to be occurring in a single step as seen from the single peak of dTG (Fig. 1). Moreover, there was no significant weight loss for PET after the active pyrolysis stage. PET pyrolysis is known to be occurring through intramolecular back-

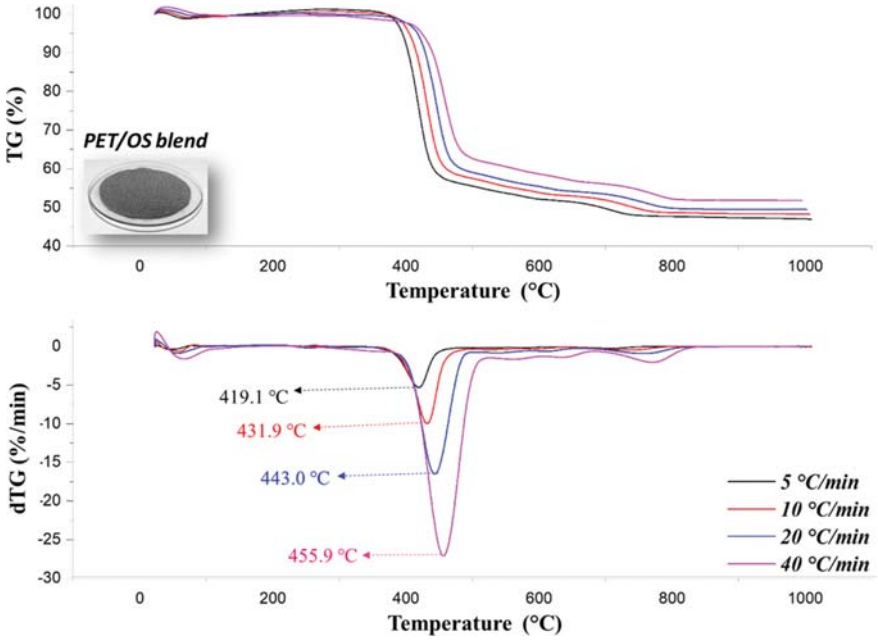

Fig. 3. Non-isothermal TG and dTG thermographs for PET/OS co-pyrolysis at different heating rates.

Table 4. Pyrolysis and co-pyrolysis characteristics of samples for each heating rate at active pyrolysis region

	β (°C/min)	T_i^* (°C)	T_{max}^{**}	T_f^{***} (°C)	R_p^{****} (%·(min·mg)$^{-1}$)
PET	5	360.2	418.5	460.1	0.804
	10	369.0	431.0	480.2	1.574
	20	374.5	443.5	495.1	3.007
	40	378.6	454.8	520.9	5.495
OS	5	315.8	445.8	560.3	0.040
	10	319.6	457.9	574.2	0.074
	20	321.2	472.8	608.2	0.149
	40	328.4	485.7	628.8	0.276
PET /OS	5	365.1	419.1	461.3	0.530
	10	367.3	431.9	475.4	0.996
	20	370.0	443.0	494.8	1.654
	40	377.5	455.9	517.1	2.764

$^*T_i$: Temperature at which the decomposition is started
$^{**}T_{max}$: Temperature at which the highest decomposition rate is observed
$^{***}T_f$: Temperature at which the decomposition is completed
$^{****}R_p$: Pyrolysis reactivity index

biting and chain scission through a β-C-H hydrogen transfer reaction during thermal degradation of the backbone [46]. Pyrolytic decomposition of PET started at around 360 °C, reaching 50% degradation at around 430 °C, and the active pyrolysis region continued up to 460 to 520 °C, depending on the heating rate. By changing heating rates from 5 to 40 °C/min, the calculated reactivity values were increased from 0.804 to 5.495%·(min·mg)$^{-1}$.

The OS pyrolysis mechanism is considered to be a complex process which includes a series of parallel reactions and highly depends on the geological origin of the OS [47-49]. However, it is convenient to say that thermal degradation of OS can be basically divided into three stages as dehydration, pyrolysis and mineral decomposition. The results show that OS pyrolysis occurred at a wider temperature range of 315-628 °C during decomposition of kerogen in OS (Fig. 2). The pyrolytic decomposition pattern consisted of three dTG peaks, and the highest peak temperature was between 445 and 485 °C, depending on the heating rate as it was perceived from the shape of the dTG curves. The reactivity values were found between 0.040 and 0.276%·(min·mg)$^{-1}$, which were relatively lower than that of PET for each heating rate. When the main pyrolysis zone ended, more than 85 wt% of residue remained in the structure. The mass loss rate became slower and stable after approximately 740 °C. During this phase, there was only a 2.50 wt% lost in the total mass. When heating was applied till the end of the thermal decomposition process, approximately 79 wt% of solid char and inorganics stayed in the solid matrix.

Regarding to co-pyrolysis, the peaks of PET and OS overlapped. The PET/OS blend did not show any considerable weight loss up to 365 °C. Only two peaks were observed clearly and the maximum sharp dTG peaks were seen at 419, 432, 443 and 456 °C for 5, 10, 20 and 40 °C/min, respectively. The solid residue was obtained between 57.2 and 61.7 wt% at the end of the degradation zones experimentally. The additive rule was applied to calculate theoretical mass loss at the end of the pyrolysis. Depending on the heating rate, the calculated solid residues were between 47.8 and 48.8 wt%. The theoretical solid residue was found less than the exper-

Table 5. Activation energy with respect to conversion degree for pyrolysis and co-pyrolysis

		Friedman		FWO		Starink		Vyazovkin
	(α)	E_a (kJ/mol)	R^2	E_a (kJ/mol)	R^2	E_a (kJ/mol)	R^2	E_a (kJ/mol)
PET	0.1	240.7	0.9978	228.4	0.9981	229.1	0.9994	228.1
	0.2	233.9	0.9945	234.1	0.9985	235.0	0.9985	232.9
	0.3	232.9	0.9969	235.0	0.9989	235.9	0.9994	231.2
	0.4	224.4	0.9980	236.4	0.9992	237.2	0.9988	233.1
	0.5	211.0	0.9993	230.5	0.9984	231.0	0.9967	210.8
	0.6	208.7	0.9958	225.4	0.9973	225.6	0.9965	208.2
	0.7	206.3	0.9997	221.9	0.9989	221.8	0.9982	205.7
	0.8	195.0	0.9977	212.3	0.9987	211.7	0.9999	195.8
	0.9	213.1	0.9960	214.2	0.9987	213.6	0.9997	212.3
	Average	218.4		226.5		226.8		217.6
OS	0.1	265.5	0.9948	272.4	0.9934	275.6	0.9929	264.0
	0.2	227.4	0.9823	240.7	0.9882	241.8	0.9871	226.9
	0.3	212.5	0.9959	225.7	0.9950	225.8	0.9945	221.4
	0.4	202.8	0.9972	218.4	0.9971	217.9	0.9967	201.9
	0.5	192.4	0.9941	207.7	0.9976	206.5	0.9973	192.8
	0.6	217.1	0.9887	207.8	0.9942	206.3	0.9934	205.5
	0.7	186.7	0.9985	208.3	0.9968	206.5	0.9964	186.1
	0.8	212.2	0.9991	206.2	0.9993	204.0	0.9991	203.9
	0.9	212.0	0.9965	211.4	0.9991	209.1	0.9991	208.9
	Average	214.3		222.1		221.5		212.4
PET/OS	0.1	204.2	0.9886	223.7	0.9939	224.3	0.9934	204.9
	0.2	199.6	0.9974	210.4	0.9977	210.2	0.9975	198.9
	0.3	206.9	0.9981	207.9	0.9991	207.5	0.9991	206.0
	0.4	207.7	0.9989	209.7	0.9993	209.3	0.9992	207.1
	0.5	203.2	0.9992	210.7	0.9993	210.2	0.9992	203.1
	0.6	209.2	0.9999	213.6	0.9998	213.2	0.9998	209.4
	0.7	204.6	0.9999	208.0	0.9996	207.3	0.9996	204.2
	0.8	210.8	0.9931	210.7	0.9998	210.0	0.9997	210.0
	0.9	194.7	0.9925	206.4	0.9996	205.4	0.9995	196.6
	Average	204.6		211.2		210.8		204.5

imental values, which indicates the synergetic effect between PET and OS during pyrolysis. As can be recognized, the blending process favors char formation during co-pyrolysis.

3. Kinetic Analysis

Pyrolysis reaction parameters are helpful to understand the microscopic reactions that occur during thermal degradation. In particular, activation energy, the minimum energy required by a chemical reaction to occur, has a critical significance for the evaluation of the kinetic scheme of thermal degradation processes. For calculation of activation energy, nine different values of the conversion degree were selected between 0 and 1 using a step size of 0.1 for each heating rate, and the activation energy was obtained from the slopes of the linear regression lines for the Friedman, FWO and Starink methods. Additionally, the Vyazovkin equation was minimized by non-linear regression to calculate activation energies. Table 5 and Fig. 4 represent the trends of the iso-conversional activation energies at each conversion degree with mean values. The regression coefficients of the models (R^2 value) were between 0.9823 and 0.9999, and they were sufficiently high enough indicating that the models were compatible with the experimental TGA data for obtaining the activation energies of the samples. As given in the table, PET had a mean activation value between 217.6 and 226.8 $kJ \cdot mol^{-1}$ depending on the kinetic models, which were quite comparable among themselves. Mean value of activation energy determined over the whole pyrolysis interval using the Starink method was slightly higher than that calculated by the Friedman, FWO and Vyazovkin models. The activation energy of PET reached its minimum value at a conversion degree of 0.8. The activation energy value slightly increased between the conversions of 0.8 and 0.9. Among the models, which use linear regression, the Starink method showed the best fit to the experimental TGA data for PET pyrolysis.

OS showed an activation energy-conversion degree dependence profile tending to decrease with a conversion degree up to 0.5. After this point, fluctuations were observed without a regular pattern. This kind of variation in the activation energy is attributed to changes in the pyrolytic degradation mechanism given the proportions of the reactive compounds as well as the possible secondary reactions [50]. The average activation energy values were calculated as 214.3, 222.1, 221.5 and 212.4 $kJ \cdot mol^{-1}$ for Friedman, FWO, Starink and Vyazovkin methods, respectively. Furthermore, the amount and content of the inorganics had a considerable effect on the kinetics. Tang et al. concluded that the crystalline structure and inorganic-organic interactions of OS have a remarkable effect on its pyrolysis. When the samples with different origins were compared, they found that the more reactive nature of OS was related to the lower amount of ash and relatively higher content of alkali metal oxides [51].

When it comes to the effect of PET blending to OS, fluctuations

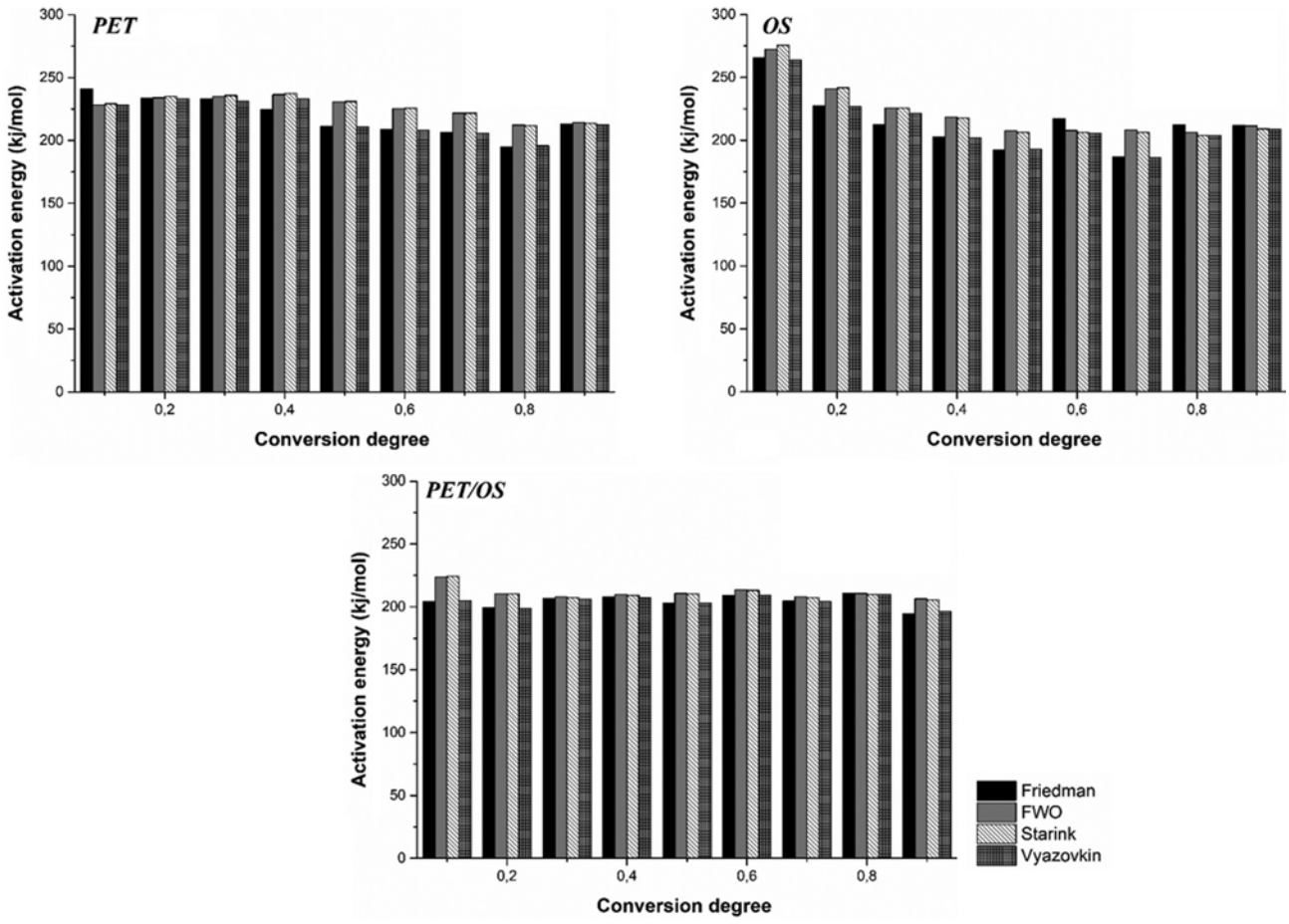

Fig. 4. The conversion degree dependence of activation energy calculated by different iso-conversional methods.

Table 6. Apparent reaction order and pre-exponential factor determined by Avrami theory*

T (°C)	PET			OS			PET/OS		
	n	A (min^{-1})	R^2	n	A (min^{-1})	R^2	n	A (min^{-1})	R^2
400	1.46	5.61×10^{15}	0.9994	0.32	1.25×10^{15}	0.9962	1.30	5.71×10^{14}	0.9989
405	1.46	6.50×10^{15}	0.9998	0.32	1.11×10^{15}	0.9981	1.30	5.59×10^{14}	0.9997
410	1.44	7.47×10^{15}	0.9980	0.33	9.55×10^{14}	0.9980	1.34	6.07×10^{14}	0.9993
415	1.36	7.23×10^{15}	0.9990	0.34	7.56×10^{14}	0.9993	1.30	6.50×10^{14}	0.9971
420	1.28	7.21×10^{15}	0.9996	0.37	6.87×10^{14}	0.9998	1.23	7.28×10^{14}	0.9893
425	1.19	6.96×10^{15}	0.9998	0.36	5.32×10^{14}	0.9986	1.22	7.29×10^{14}	0.9934
430	1.17	6.64×10^{15}	0.9989	0.38	4.49×10^{14}	0.9972	1.19	7.61×10^{14}	0.9954
435	1.10	6.39×10^{15}	0.9988	0.39	3.88×10^{14}	0.9972	1.18	6.75×10^{14}	0.9990
440	1.06	5.66×10^{15}	0.9997	0.41	3.43×10^{14}	0.9991	1.12	3.98×10^{14}	0.9963
445	0.99	4.07×10^{15}	0.9994	0.43	3.05×10^{14}	0.9996	1.08	3.73×10^{14}	0.9911
450	0.96	2.65×10^{15}	0.9981	0.44	2.59×10^{14}	0.9997	0.98	2.07×10^{14}	0.9851
455	0.92	1.32×10^{15}	0.9999	0.44	2.13×10^{14}	0.9970	0.90	1.84×10^{14}	0.9890
460	1.07	1.26×10^{15}	0.9799	0.43	1.70×10^{14}	0.9986	1.07	1.11×10^{14}	0.9865

*Calculations based on activation energy values found by Friedman method at a heating rate of 10 °C/min

in activation energies were observed by increased conversion degrees for the co-pyrolysis process. These irregular trends in the activation energy values were attributed to the complex reaction schemes, which imply parallel, competitive and complex reactions during pyrolytic degradation of PET/OS. Hence, there was a competitive relationship between the mechanisms that led the activation energies to decrease and increase due to the heterogeneous nature of the precursors. The mean activation energy of the co-pyrolysis process was lower than the values obtained from the pyrolysis process of single components. This observation shows that there may be a synergetic effect during the reactions occurring in OS and PET fragments. The lower activation energy during co-pyrolysis indicates that co-pyrolysis was easier to facilitate pyrolytic conversion. Therefore, co-pyrolysis of OS and PET should have created feasible thermochemical conversion processes once they were used as raw materials to produce energy or chemical feedstock. Pyrolysis of PET produced abundant free radicals that then promoted the thermal degradation of a small proportion of OS, causing a lower mean activation energy value. Similarly, based on the results of OS and PET, all activation energy values had high regression coefficients in the narrow range of 0.9886-0.9999, reflecting that the co-pyrolysis results of PET/OS were credible. Minor variations among the kinetic models mainly resulted from the calculations and approximations that were used to solve the temperature integral of the methods.

The pre-exponential factor (A) and reaction order (n) in a certain temperature range (between 400 and 460 °C) were also calculated for characterization of the pyrolysis and co-pyrolysis characteristics of OS, PET and their blend. The results of the apparent reaction order and pre-exponential factor determined by Avrami's theory are given in Table 6. Depending on the high value of the regression coefficients, it could be concluded that the calculated reaction order and pre-exponential coefficient for OS pyrolysis, PET pyrolysis and PET/OS co-pyrolysis performed satisfyingly linear regressions through the Avrami theory. Based on the findings, the reaction order of OS was estimated to be lower than that of PET during pyrolysis. The reaction order of PET/OS varied with increased temperature to illustrate the complexity of the co-pyrolysis of the investigated samples, which was similar to variation trend of the activation energy. It is convenient to say that PET domi-

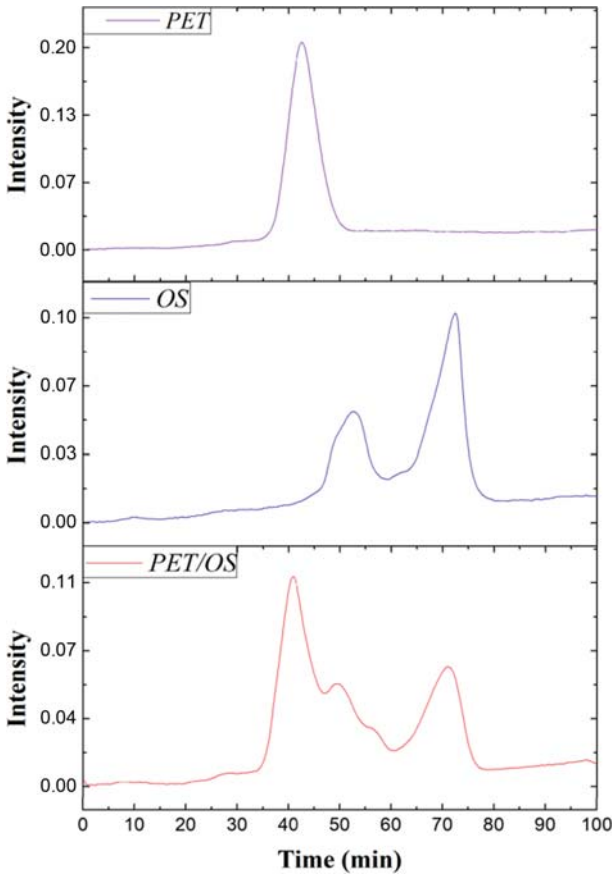

Fig. 5. Gram-schmidt curves for PET, OS pyrolysis and PET/OS co-pyrolysis.

nated co-pyrolysis depending on the reaction orders at the active pyrolysis stage. Overall, the mean values of the apparent reaction order for OS, PET and PET/OS between 400 and 460 °C were approximately 0.38, 1.18 and 1.17, respectively.

The pre-exponential factor (A) may be used to characterize the reaction speed in the pyrolysis process. According to the results, the pre-exponential factor varied at different temperatures for OS, PET and their blends through thermal decomposition. The pre-exponential factor calculated for OS pyrolysis decreased from 1.25×10^{15} to 1.70×10^{14} with increasing temperature. The decrease in the pre-exponential factor indicated a decrease in collision intensity. For PET, the early stages of pyrolysis tended to increase the pre-exponential factor up to 7.47×10^{15} but then caused a considerable fall. In thermal degradation processes, the low pre-exponential factor values ($A<10^9\ s^{-1}$) indicate surface reactions in most cases, but if the reactions are not dependent on surface area, low pre-exponential factors may indicate a closed complex. On the other hand, high pre-exponential factors ($A\geq10^9\ s^{-1}$) often point out a simple complex. In particular, when the values of pre-exponential factors are between 10^{10} and $10^{12}\ s^{-1}$, the activated complex is likely restricted in rotation in comparison to the initial reagent. For the unimolecular case, the complex is expected to expand by size and interact more intensely with its neighbors [52]. As may be observed in Table 6, pre-exponential factors for OS pyrolysis, PET pyrolysis and PET/OS co-pyrolysis had similar numerical values around the order of 10^{14} and $10^{15}\ s^{-1}$. However, comparing the co-pyrolysis results to the pre-exponential factors of the single component pyrolysis processes, the synergetic effects could be concluded to be due to the fluctuations of collisions. Variation in pre-exponential values with temperature during PET/OS co-pyrolysis clearly indicated complex reaction mechanisms because of the compositional differences of OS and PET and their complex radical interactions.

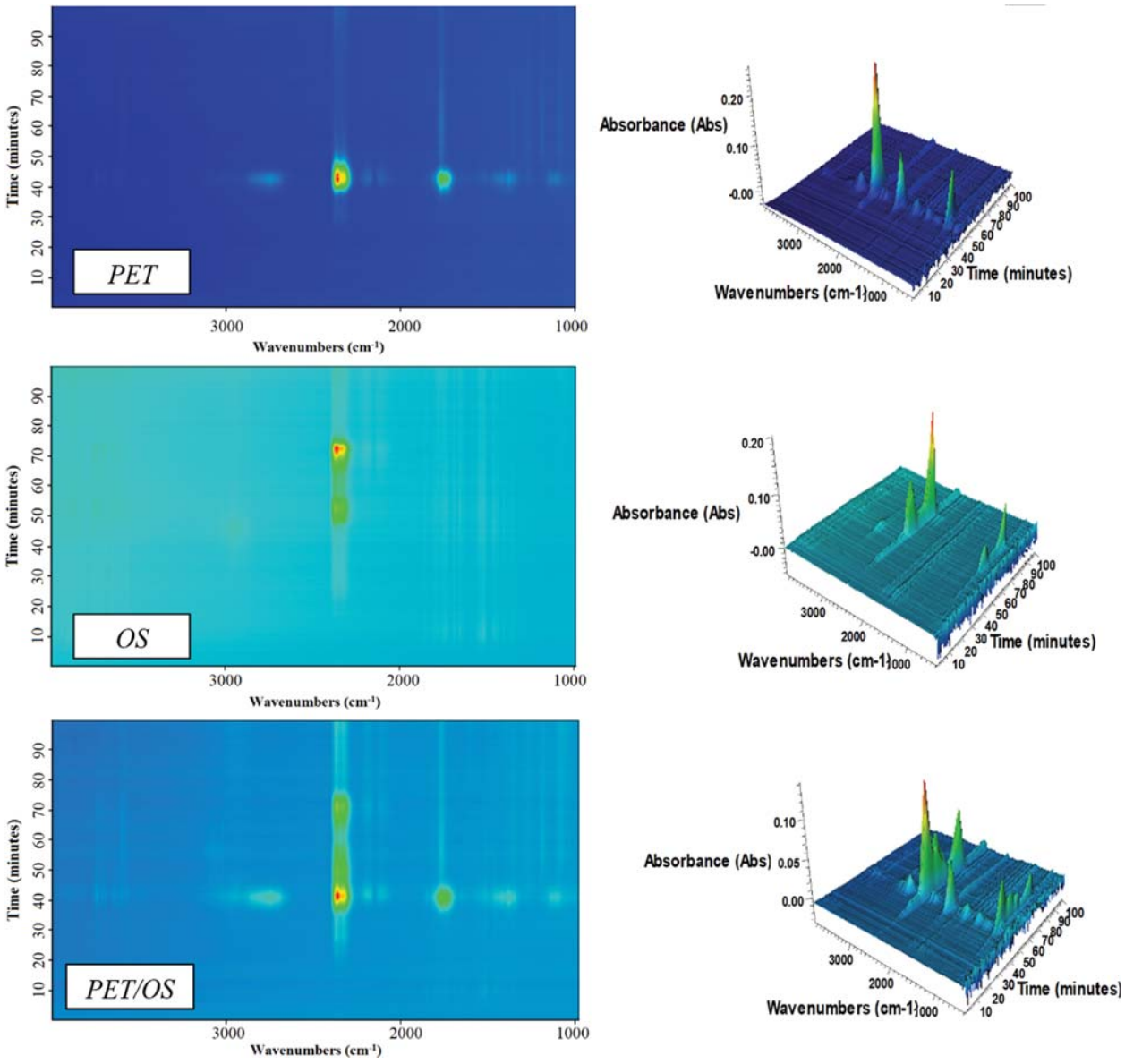

Fig. 6. The evolution of gases during the pyrolysis and co-pyrolysis process.

4. Evolved Gas Analysis

Although data obtained TGA gives beneficial kinetic information on pyrolysis reactions, combined thermal and spectroscopic techniques such as TGA/FT-IR are practical to explain the evolved gasses during pyrolysis reaction at the same time [53]. With the purpose of a further understanding for the mechanisms of pyrolysis and co-pyrolysis, the spectra of gaseous species evolved during pyrolytic degradation of OS, PET and their blends were recorded dynamically, and the results were processed by the OMNIC software. Gram-Schmidt (GS) curves obtained in the pyrolysis and co-pyrolysis experiments are graphically presented in Fig. 5. The GS curves exhibited a total change in the IR signal relative to the initial state and hence provided information on the total IR absorbance of the evolved components over the entire spectra. The curves correlated with a selected heating rate of 10 °C/min over the temperature range from 25 (at time=0 min) to 1,000 °C. The GS curve of OS revealed two weight loss steps, while PET showed a single step which was similar to the dTG curves. Like the case of OS and PET, GS curve of PET/OS was in accordance with the dTG curve. Qualitative information about the evolved gases was also attained based on the location of the infrared absorption bands given in both 3-dimensional spectra which are shown in Fig. 6. Additionally, the instantaneous FT-IR spectra corresponding to gas evolved at the maximum pyrolysis rate are shown in Fig. 7.

During pyrolysis of OS, kerogen degrades into shale oil, gas, water and carbonaceous residues through covalent bond cleavage and polycondensation (condensation, cyclization, addition) reactions with increasing temperature via pyrolytic decomposition. As a consequence of such reactions, hydrocarbons with low molecular weight are released, and carbonaceous char including inorganics is formed simultaneously [54]. Evolution of hydrocarbons is due to decomposition of kerogen which is in the form of a three-dimensional network of disordered amorphous polymers. Presence of asymmetrical C=O stretching vibrations at 2,500-2,250 cm^{-1} and bending vibrations at 730-580 cm^{-1} in the spectra of OS indicated the release of CO_2 because of the cracking of the carbonyl and carboxyl groups from the matrix. The release of CO_2 during active pyrolysis starts from approximately 315 °C and continues up to the end of thermal decomposition process, including the gasification stage. Although mass loss was not significant after the pyrolysis stage, CO_2 release exhibited a sharp increment after approximately 630 °C up to 815 °C. Slightly observable aliphatic C-H stretching vibrations at 3,030-2,850 cm^{-1} in the 3-D spectra of OS showed a release of methane also because of the release of saturated hydrocarbons including the methyl group. Likewise, the OS, PET spectra also showed the presence of asymmetrical C=O stretching vibrations at 2,500-2,250 cm^{-1} and bending vibrations at 730-580 cm^{-1} due to CO_2 evolution. Additionally, bands between 2,250 and 2,000 cm^{-1} on the PET spectrum belonged to the C-O stretching vibration that indicated CO formation and vibrations between 1,900 and 1,650 cm^{-1} were attributed to C=O stretching which originated from carboxylic acids, aldehydes, and ketones. Co-pyrolysis of OS and PET showed overlapping of the peak positions of OS and PET pyrolysis. However, peak intensities were changed, which was mainly observed in CO_2 evolution. These changes in the CO_2 evolution mechanism may be attributed to promotion of the breakage of main covalent bonds during co-pyrolysis.

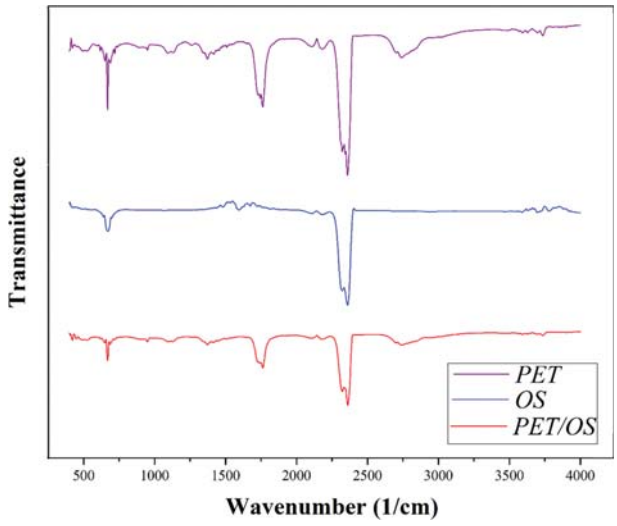

Fig. 7. Instantaneous FT-IR spectra corresponding to gas evolved at maximum pyrolysis rate at a heating rate of 10 °C/min.

CONCLUSIONS

Pyrolysis and co-pyrolysis characteristics of the OS and PET were studied through TGA/FT-IR. The kinetic parameters of the pyrolysis and co-pyrolysis processes were calculated by four different non-isothermal kinetic methods. In comparison to the pyrolysis of individual materials, the average activation energy of co-pyrolysis declined, which indicates that PET exerted synergetic effect on pyrolysis of OS. The kinetic models that were used were found to be validated with the obtained data to describe the pyrolytic and co-pyrolytic degradation mechanisms. Overall, these findings represent a novel insight into co-pyrolysis of OS with PET and may serve as a valuable reference for shale oil production, prediction of the distributions for final products and supplying data for optimizing co-pyrolysis reactors, as well as resourceful utilization of polymeric wastes.

REFERENCES

1. H. C. Ong, W.-H. Chen, A. Farooq, Y. Y. Gan, K. T. Lee and V. Ashokkumar, *Renew. Sust. Energy Rev.*, **113**, 109266 (2019).
2. A. Tahmasebi, K. Maliutina and J. Yu, *Korean J. Chem. Eng.*, **36**, 393 (2019).
3. Y. J. Bae, C. Ryu, J.-K. Jeon, J. Park, D. J. Suh, Y.-W. Suh, D. Chang and Y.-K. Park, *Bioresour. Technol.*, **102**, 3512 (2011).
4. Y.-M. Kim, H. W. Lee, S. H. Jang, J. Jeong, S. Ryu, S.-C. Jung and Y.-K. Park, *Korean J. Chem. Eng.*, **37**, 493 (2020).
5. S. Siramard, L. Lin, C. Zhang, D. Lai, S. Cheng and G. Xu, *Fuel Process. Technol.*, **148**, 248 (2016).
6. H. Jiang, S. Deng, J. Chen, M. Zhang, S. Li, Y. Shao, J. Yang and J. Li, *Energy Convers. Manage.*, **143**, 505 (2017).
7. C. Culin, K. Tente, A. Konist, B. Maaten, L. Loo, E. Suuberg and I. Külaots, *Oil Shale*, **36**, 353 (2019).
8. Z. Chang, M. Chu, C. Zhang, S. Bai, H. Lin and L. Ma, *J. Anal.*

Appl. Pyrolysis, **130**, 269 (2018).
9. M. Kılıç, A. E. Pütün, B. B. Uzun and E. Pütün, *Energy Convers. Manage.*, **78**, 461 (2014).
10. P. A. Bozkurt, O. Tosun and M. Canel, *J. Energy Inst.*, **90**, 355 (2017).
11. J. Tu and J. J. Sheng, *J. Taiwan Inst. Chem. E.*, **106**, 169 (2020).
12. Z. Chang, M. Chu, C. Zhang, S. Bai, H. Lin and L. Ma, *Korean J. Chem. Eng.*, **34**, 3111 (2017).
13. L. Al-Makhadmeh, J. Maier, M. Al-Harahsheh and G. Scheffknecht, *Fuel*, **103**, 421 (2013).
14. A. Al-Harahsheh, M. Al-Harahsheh, A. Al-Otoom and M. Allawzi, *Fuel Process. Technol.*, **90**, 818 (2009).
15. M. W. Amer, J. S. A. Alhesan, M. Marshall, A. M. Awwad and O. S. Al-Ayed, *J. Anal. Appl. Pyrolysis*, **140**, 219 (2019).
16. J. Shah and M. R. Jan, *J. Taiwan Inst. Chem. E.*, **51**, 96 (2015).
17. H. W. Ryu, Y. F. Tsang, H. W. Lee, J. Jae, S.-C. Jung, S. S. Lam, E. D. Park and Y.-K. Park, *Chem. Eng. J.*, **373**, 375 (2019).
18. L. Zhou, T. Luo and Q. Huang, *Energy Convers. Manage.*, **50**, 705 (2009).
19. X. Wang, D. Ma, Q. Jin, S. Deng, H. Stančin, H. Tan and H. Mikulčić, *Fuel Process. Technol.*, **194**, 106127. (2019).
20. S. Park, J. Jae, A. Farooq, E. E. Kwon, E. D. Park, J.-M. Ha, S.-C. Jung and Y.-K. Park, *Appl. Energy*, **255**, 113801 (2019).
21. A. Aboulkas and M. Nadifiyine, *Fuel Process. Technol.*, **89**, 1000 (2008).
22. L. Ballice, M. Yüksel, M. Sağlam, R. Reimert and H. Schulz, *Fuel*, **77**, 1431 (1998).
23. J. Zhang, Z. Zhong, B. Zhang, Z. Xue, F. Guo and J. Wang, *Clean Technol. Environ. Policy*, **18**, 1621 (2016).
24. Z. Till, T. Varga, J. Sója, N. Miskolczi and T. Chován, *Energy Convers. Manage.*, **173**, 320 (2018).
25. Z. Zhang, M. Zhu and D. Zhang, *Appl. Energy*, **220**, 87 (2018).
26. E. A. Williams and P. T. Williams, *J. Chem. Technol. Biotechnol.*, **70**, 9 (1997).
27. G. Özsin, and A. E. Pütün, *J. Clean. Prod.*, **205**, 1127 (2018).
28. T. Yoshioka, G. Grause, C. Eger, W. Kaminsky and A. Okuwaki, *Polym. Degrad. Stabil.*, **86**, 499 (2004).
29. Ö. Çepelioğullar and A. E. Pütün, *J. Anal. Appl. Pyrolysis*, **110**, 363 (2014).
30. J. M. Park, S. Keel, J. Yun, J. H. Yun and S.-S. Lee, *Korean J. Chem. Eng.*, **34**, 2204 (2017).
31. F. Yang, Q. Yu, H. Xie, Z. Zuo, L. Hou and Q. Qin, *Korean J. Chem. Eng.*, **35**, 1626 (2018).
32. G. Özsin and A. E. Pütün, *Korean J. Chem. Eng.*, **35**, 428 (2018).
33. P. Parthasarathy, H. S. Choi, J. G. Hwang and H. C. Park, *Korean J. Chem. Eng.*, **34**, 1678 (2017).
34. A. Boytsova, N. Kondrasheva and J. Ancheyta, *Energy Fuels*, **32**, 1132 (2018).
35. C. Yao, H. Tian, Z. Hu, Y. Yin, D. Chen and X. Yan, *Korean J. Chem. Eng.*, **35**, 511 (2018).
36. Y. Lin, Y. Liao, Z. Yu, S. Fang, Y. Lin, Y. Fan, X. Peng and X. Ma, *Energy Convers. Manage.*, **118**, 345 (2016).
37. J. Huang, J. Liu, J. Chen, W. Xie, J. Kuo, X. Lu, K. Chang, S. Wen, G. Sun, H. Cai, M. Buyukada and F. Evrendilek, *Bioresour. Technol.*, **266**, 389 (2018).
38. H.L. Friedman, *J. Polym. Sci. Pol. Sym. C*, **6**, 183 (1964).
39. J. H. Flynn and L. A. Wall, *J. Res. Nat. Bur. Stand*, **70**, 487 (1966).
40. T. Ozawa, *Bull. Chem. Soc. Jpn.*, **38**, 1881 (1965).
41. M. Starink, *Thermochim. Acta*, **288**, 97 (1996).
42. S. Vyazovkin, *J. Therm. Anal.*, **49**, 1493 (1997).
43. S. Niu, Y. Zhou, H. Yu, C. Lu and K. Han, *Energy Convers. Manage.*, **149**, 495 (2017).
44. X. Wang, S. Deng, H. Tan, A. Adeosun, M. Vujanović, F. Yang and N. Duić, *Energy Convers. Manage.*, **118**, 399 (2016).
45. D. Lai, G. Zhang and G. Xu. *Fuel Process. Technol.*, **158**, 191 (2017).
46. B. Holland and J. Hay, *Polymer*, **43**, 1835 (2002).
47. P. T. Williams and N. Ahmad, *Appl. Energy*, **66**, 113 (2000).
48. J. Jaber, S. Probert and P. Williams, *Energy*, **24**, 761 (1999).
49. P. T. Williams and N. Ahmad, *Fuel*, **78**, 653 (1999).
50. Z. Chen, Q. Zhu, X. Wang, B. Xiao and S. Liu, *Energy Convers. Manage.*, **105**, 251 (2015).
51. L. Tang, Y. Yan, Y. Meng, J. Wang, P. Jiang, C. H. Pang and T. Wu, *Energy Procedia*, **158**, 1694 (2019).
52. X. Yuan, T. He, H. Cao and Q. Yuan, *Renewable Energy*, **107**, 489 (2017).
53. S. Zhao, M. Liu, L. Zhao and J. Lu, *Korean J. Chem. Eng.*, **34**, 3077 (2017).
54. M. Dai, Z. Yu, S. Fang and X. Ma, *Energy Convers. Manage.*, **192**, 1 (2019).